Fabrication of elliptically figured mirror for focusing hard x rays to size less than 50 nm

Hirokatsu Yumoto,[a] Hidekazu Mimura, Satoshi Matsuyama, and Hideyuki Hara
Department of Precision Science and Technology, Graduate School of Engineering, Osaka University, 2-1 Yamada-oka, Suita, Osaka 565-0871, Japan

Kazuya Yamamura
Research Center for Ultra-Precision Science and Technology, Graduate School of Engineering, Osaka University, 2-1 Yamada-oka, Suita, Osaka 565-0871, Japan

Yasuhisa Sano and Kazumasa Ueno
Department of Precision Science and Technology, Graduate School of Engineering, Osaka University, 2-1 Yamada-oka, Suita, Osaka 565-0871, Japan

Katsuyoshi Endo and Yuzo Mori
Research Center for Ultra-Precision Science and Technology, Graduate School of Engineering, Osaka University, 2-1 Yamada-oka, Suita, Osaka 565-0871, Japan

Makina Yabashi
SPring-8/Japan Synchrotron Radiation Research Institute (JASRI), 1-1-1 Kouto, Mikazuki, Hyogo 679-5148, Japan

Yoshinori Nishino, Kenji Tamasaku, and Tetsuya Ishikawa
SPring-8/RIKEN, 1-1-1 Kouto, Mikazuki, Hyogo 679-5148, Japan

Kazuto Yamauchi
Department of Precision Science and Technology, Graduate School of Engineering, Osaka University, 2-1 Yamada-oka, Suita, Osaka 565-0871, Japan

(Received 28 December 2004; accepted 5 February 2005; published online 7 June 2005)

In this study, we designed, fabricated, and evaluated a hard x-ray focusing mirror having an ideally focused beam with a full width at half maximum in the intensity profile of 36 nm at an x-ray energy of 15 keV. The designed elliptically curved shape was fabricated by a computer-controlled fabrication system using plasma chemical vaporization machining and elastic emission machining, on the basis of surface profiles accurately measured by combining microstitching interferometry with relative angle determinable stitching interferometry. A platinum-coated surface was employed for hard x-ray focusing with a large numerical aperture. Line-focusing tests on the fabricated elliptical mirror are carried out at the 1-km-long beamline of SPring-8. A full width at half maximum of 40 nm was achieved in the focused beam intensity profile under the best focus conditions. © *2005 American Institute of Physics.* [DOI: 10.1063/1.1922827]

I. INTRODUCTION

Highly brilliant and coherent x-ray beams are provided by undulators at third-generation synchrotron radiation sources. The exceptional brilliant and coherent x rays provided by undulators at third-generation synchrotron sources has revolutionized nondestructive analysis of characteristics such as crystallographic structures, elemental composition, and chemical bonding in wide-range materials. Focused hard x-ray beams are employed for various scanning-type microscopes to give precise spatial information on the above-mentioned characteristics. There are many types of hard x-ray focusing device that utilize refraction, reflection, and diffraction optics. These techniques have been advanced on the basis of ultraprecise optics coupled with highly brilliant and/or coherent sources. Most of hard x-ray focusing approaches have the ability to focus hard x rays down to the submicron level.[1–5] However, the inherently nondispersive nature of total external reflection mirrors for x-ray microfocusing is most attractive when we consider spectroscopic applications that usually require broad bandpass or energy tunability. For this purpose, Kirkpatrick–Baez (K–B) mirrors are being developed. This classical method utilizes two concave mirrors at a glancing angle to collect and focus x rays in both vertical and horizontal axes for x-ray microfocusing. However, microfocusing mirrors for x rays demand figure perfection with subnanometer-height errors as well as a surface roughness of less than ~0.3 nm rms. Until quite recently, this mirror quality has only been possible for spherical or flat figures, but not for elliptical figures required for K–B mirrors. Some researchers have developed benders for making elliptical figures from flat figures[6] or have used a differential deposition technique for modifying the figure of cylindrical substrates.[7]

[a]Electronic mail: yumoto@up.prec.eng.osaka-u.ac.jp

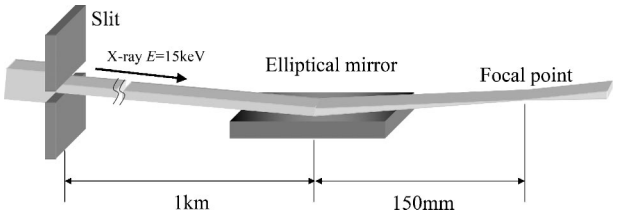

FIG. 1. Schematic drawing of the layout of optical system for line focusing with a single reflective mirror.

Directly figured elliptical mirrors have many advantages such as the overwhelming ease of alignment and short setup time. Plasma chemical vaporization machining (PCVM) and elastic emission machining (EEM) can figure mirror surfaces with peak-to-valley accuracies as better than 1 nm and lateral resolutions close to 0.1 mm.[8] In our previous study, computer-controlled PCVM and EEM were used in the fabrication of elliptical mirrors for the submicron focusing of hard x rays.[4,5,9–11] These mirrors were confirmed at the 1 -km-long beam line (BL29XUL) of SPring-8 to have diffraction-limited performances. The designed full width at half maximum (FWHM) 90 nm was achieved.[5]

To realize a smaller focal size, more steeply curved elliptical mirrors having a larger glancing angle are necessary, to improve the numerical aperture (NA). In this study, we designed and fabricated a hard x-ray focusing mirror having a designed focused beam with a FWHM of intensity profile of 36 nm. A platinum-coated surface having a relatively large critical angle is employed for large NA optical system design. A line-focusing test was also performed at the 1-km-long beam line (BL29XUL) of SPring-8 because the available incident x ray had been confirmed to have sufficient coherence to evaluate ultraprecise mirrors.[12]

One of the main fabrication obstacles was the need for a surface figure profiler for measuring the steeply curved surface profile. Relative angle determinable stitching interferometry (RADSI)[13] was developed to measure the surface profile. The high-quality elliptically curved surface was manufactured by the computer-controlled figuring system using PCVM and EEM, in which surface profiles are accurately measured by combining both microstitching interferometry (MSI)[14] with RADSI. The wire scanning method was employed for measuring the intensity distribution profiles of the focused beam at the focal plane. Nearly diffraction limited performance with a FWHM of 40 nm was realized in the focal beam profile under the best focusing conditions.

II. DESIGN OF SURFACE PROFILE OF HARD X-RAY FOCUSING MIRROR

Figure 1 shows a schematic drawing of the layout of an optical system for line focusing with a single reflective mirror. Consideration of the geometrical demagnification leads to the following equation regarding focal spot size (D_1):

$$D_1 = \nu/u \cdot d. \tag{1}$$

Here, u is the distance from the synchrotron source to the mirror center, ν is the focal length, and d is an object size at the source. In addtion, when the incident ray is perfectly coherent, the diffraction-limited focal spot size is approximately determined by the following equation in the wave-optical theory:

$$D_2 = \lambda/\mathrm{NA} = \lambda \times 2 \cdot \nu/(L \cdot \sin\theta). \tag{2}$$

Here, λ is the wavelength of the light, NA is the numerical aperture, L is the mirror length, and θ is the glancing angle of an incident beam. The calculated demagnification size (D_1) should be smaller than the diffraction-limited focal size (D_2) to obtain the optimum performances of focusing mirrors.

Equation (1) shows that the longer the object distance u, the smaller the focal size obtained. In this study, a focusing test was carried out at the 1-km-long beamline (BL29XUL) of SPring-8. The geometrical relationships between the x-ray source, mirror, and focusing position are determined on the assumption of beamline geometry. When ν, u, and d are selected to be 150 mm, 1 km, and 100 μm, respectively, in Eq. (1), D_1 is calculated to be only 15 nm. This calculation result denotes that a nanofocused hard x-ray beam with a size less than 50 nm is feasible at this beamline.

TABLE I. Parameters of the designed elliptical mirror.

Substrate material	CZ-(111) Si single crystal
Surface coating	Pt
Effective mirror size in longitudinal direction	90 mm
Focal length	150 mm
Length of ellipse	500.075 m
Breadth of ellipse	44.7 mm
Glancing angle on optical axis	3.65 mrad
Maximum glancing angle	4.47 mrad
Acceptance width	329 μm

The designed surface profile is a partial profile of an elliptic function in which one focal point is the position of an incident slit as an x-ray source and the other focal point is the position where x rays collect. Table I shows the parameters of the ellipse function. By employing a heavy metal surface as a reflective surface, the incident ray can totally reflect at a large glancing angle. In this study, the silicon substrate surface was coated by platinum. The mirror length is 90 mm. The maximum incident angle is 4.47 mrad, which is equal to the critical angle of the platinum surface at approximately 18 keV. The average incident angle is 3.65 mrad. The focal length is set to be 150 mm to provide a sufficiently long working distance in a microscope system, in which the fabricated mirror will be used for realizing two-dimensional focusing at the K-B arrangement. Figure 2 shows the designed elliptical profile. When λ is 0.8 Å and the determined values are assigned in the coefficients of Eq. (2), D_2 is calculated to be 73 nm. Figure 3 shows the predicted intensity profile at the focal plane, which is obtained by a wave-optical simulator coded on the basis of the Fresnel–Kirchhoff diffraction integral theory.[15] The optical system in the simulation is the same as that designed for the mirror surface profile. Incident slit width and x-ray energy are selected to be 100 μm and 15 keV, respectively. The transverse coherence length at the incident slit was assumed to be 50 μm. This calculated intensity profile denotes the obtainable intensity profile under the diffraction limited fo-

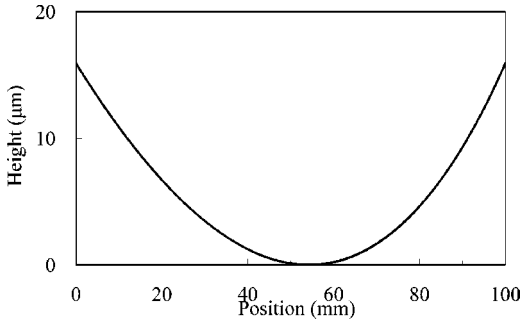

FIG. 2. Designed elliptical profile of the mirror for nanofocusing of hard x ray.

cusing conditions. The FWHM and the width between the first two minima are 36 and 68 nm, respectively. The latter width is almost the same as that easily predicted using Eq. (2).

III. FABRICATION OF HARD X-RAY FOCUSING MIRROR

The x-ray mirror was fabricated by figuring a Si (111) substrate surface shape into a designated one with required accuracy for nanofocusing, using computer-controlled EEM and PCVM and then by coating platinum on the figured surface area, using a scanning-type platinum deposition system.[7]

In our fabrication system, metrology plays an important role because computer-controlled figuring is carried out on the basis of measured surface profiles. We developed MSI, in which microscopic and large-area phase-shifting interferometers are utilized, to measure the surface profiles of x-ray mirrors with a reproducibility of less than 1 nm (peak-to-valley) and with a spatial resolution of approximately 20 μm.[14] Total-reflection x-ray mirrors have such a steep rectangular shape that the number of stitches in the longitudinal direction exceeds 30. A Fizeau interferometer, which can measure a large-area profile in one shot, is used to compensate for the stitching angles. Only MSI has currently demonstrated sufficient accuracy for measurement of ultraprecise prefabricated flat and elliptical mirror profiles. In previous studies regarding the development of focusing mirrors, the realization of diffraction limited line focusing verified the effectiveness of MSI.

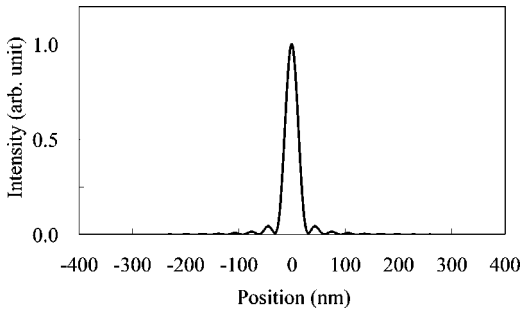

FIG. 3. Predicted intensity profile at focal plane, which is obtained by wave-optical simulator coded on the basis of the Fresnel–Kirchhoff diffraction integral theory.

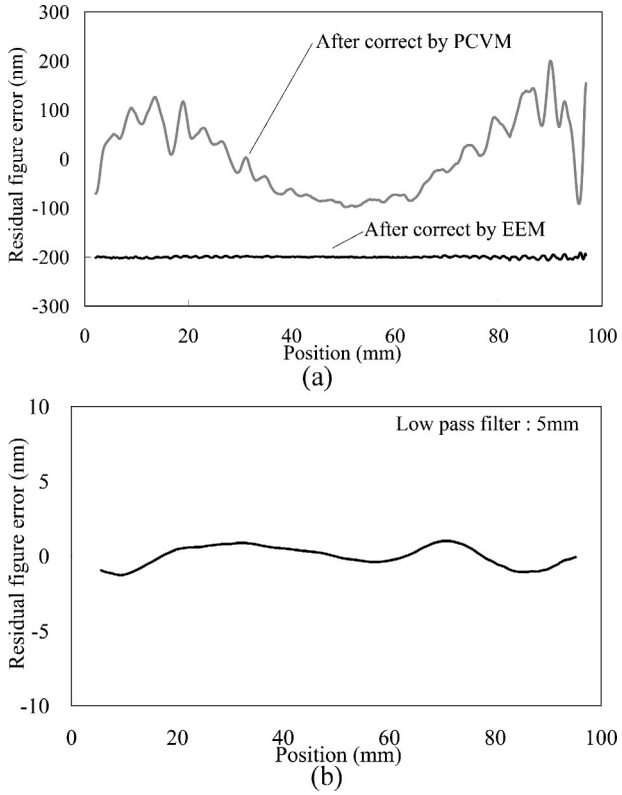

FIG. 4. Residual figure error profiles of the fabricated mirror after PCVM figuring and EEM figuring 5 mm low pass filtered profile (b)shows that the figure error at relatively long spatial wavelength ranges is removed at the required degree of figure accuracy.

For this study, designed profile curvature was so large that it could not be measured in one shot using a Fizeau interferometer and MSI could not satisfy the required measurement accuracy at a long spatial wavelength range. RADSI, using a Fizeau interferometer, was developed to measure the steeply curved profile at a required accuracy. In the new stitching system, several partial profiles covering the entire area, which are measured using the Fizeau interferometer, are stitched to create an entire surface profile, utilizing the stitching angles determined not by the general method using a common area between neighboring shots, but by the method using the mirror's tilt angles measured at the acquisitions of figure profiles. To evaluate the performance of RADSI in the case of measuring the designed profile, the two surface profiles were measured, placing the mirror having the same curvature as the designed one normally and upside down. The peak-to-valley distance of the differential profiles between the two identically measured profiles is confirmed to be only 3 nm.

In addition, the relationship between figure error characteristics and focusing property has been investigated using a wave-optical simulator. The obtained results indicate that the figure errors characterized in the spatial wavelength range from 4 to 50 mm affect the shape of the focused beam profile.[13] To realize the ideal beam focal size, the figure accuracy needs to be at least 4 nm (peak-to-valley) in this spatial wavelength range.

In this study, with an emphasis on figure correction in the middle and long spatial wavelengths, the mirror was fab-

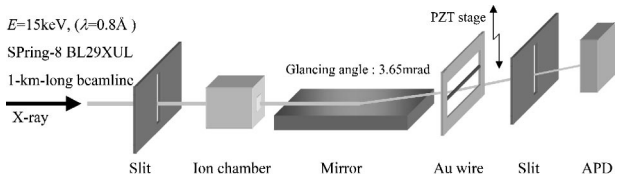

FIG. 5. Schematic drawing of experimental setup for measuring intensity profiles of nanoline-focused beams.

ricated to demonstrate the performance of the RADSI and simulation results. Figure 4 shows residual figure error profiles after each figuring. In the first step using PCVM, a peak-to-valley figure error of approximately 200 nm or less is achieved. After the final correction using EEM, the peak-to-valley figure error is 6 nm. However, the 5 mm low pass filtered profile shows that the figure error at relatively long spatial wavelength ranges is removed at the required degree of figure accuracy.

Finally, platinum deposition was performed using the electron beam evaporation technique. An initial binder coat of Cr is deposited. In the deposition chamber, the mirror surface is passed over a small aperture located approximately 400 mm above the evaporation source, while the source power is controlled by a feedback system to maintain the measured deposition rate. As many as 500 passes were required to achieve a thickness of 40 nm over the entire area.

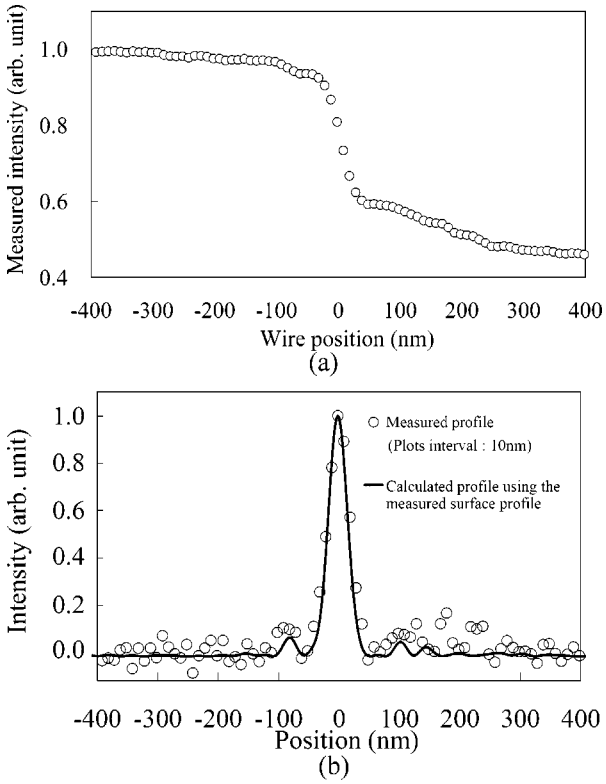

FIG. 6. Intensity profile measured under best focusing conditions shown in (a) and its differential curve corresponding to focal beam profile shown in (b) at an x-ray energy of 15 keV.

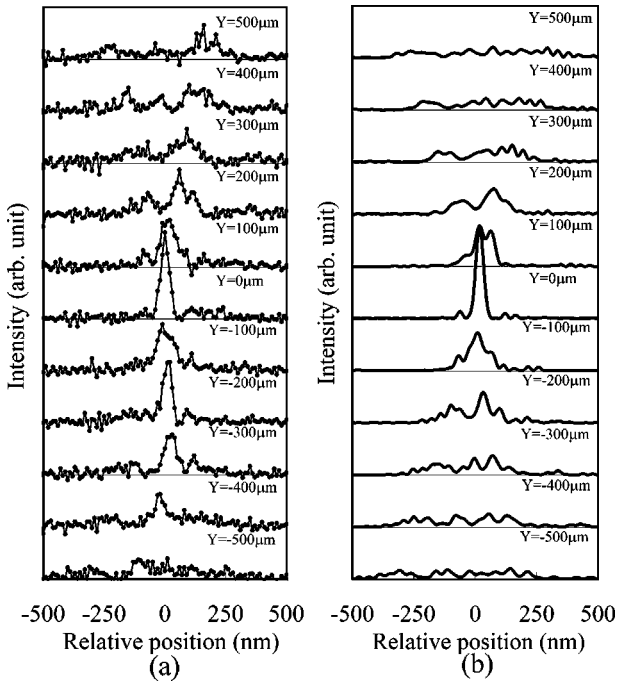

FIG. 7. Cross-sectional intensity profiles every 100 μm in the beam direction over a ~500 μm range from focal plane: (a) measured cross-sectional intensity profiles and (b) wave optically predicted cross-sectional intensity profiles using the measured surface profile.

The surface profiles before and after Pt coating were compared and evaluated to be in good agreement at the subnanometer level.

IV. LINE-FOCUSING TEST

The line-focusing test was performed at the 1-km-long beamline (BL29XUL) of SPring-8. Monochromatic x rays at 15 keV were prepared with the cryogenic-cooled double-crystal Si (111) monochromator and guided to an experimental hutch located 1 km far from the monochromator. Figure 5 shows a schematic drawing of the experimental setup for measuring the intensity profiles of the nanoline-focused beams. To ensure good vibrational damping, both the wire scanning stage and mirror holder were mounted on the same rigidly structured table set on one of the goniometers (KOUZU, KTG-15) of the high-precision diffractometer system installed in the experimental hutch. A piezoactuated translation stage (PI, P-733) enabled wire scanning at a 10 nm increments. A gold wire having a diameter of 200 μm was placed at the designed focal position. An avalanche photodiode detector placed behind the wire was used for measuring beam intensity. All alignment parameters except for the glancing angle were preadjusted when the mirror was positioned. Precise adjustment of the glancing angle was performed until the best focusing had been achieved, while monitoring the intensity profile.

Figures 6(a) and 6(b) show the intensity profile measured under the best focusing conditions and its differential curve corresponding to the focal beam profile, respectively. Figure 6(b) also shows the simulated beam profile obtained by calculating the Fresnel–Kirchhoff integral using the measured mirror figure as the boundary condition. The measured

profile has completely raw data without any compensation taking the transmission effect at the gold wire edge into account. The FWHM of the focal line is as narrow as 40 nm. The fairly good agreement between the measured and calculated profiles indicates the effectiveness of metrology in fabricating the mirror and predicting focusing performance.

The wave-optical property of the present mirror is more clearly seen when we measure the beam profiles out of the focal plane. Figure 7(a) shows the cross-sectional intensity profiles measured every 100 μm in the beam direction over a $\sim$500 μm range from the focal plane, while the corresponding profiles wave optically predicted using the measured surface profile are shown in Figure 7(b). The constructive and destructive interferences observed near the beam waist, which agree fairly well with the calculation, indicate that the present focusing is nearly diffraction limited. The focused beam size (FWHM) is clarified to be less than 50 nm within a displacement of 50 μm along the beam direction. The relatively long depth of the focus is one of the reasons the beam profile could be measured by the wire scanning method with 200 μm. By preparing one more elliptical mirror, a two-dimensionally focused x-ray beam having a focal size of approximately 50 nm (FWHM) is feasible.

ACKNOWLEDGMENT

This research was supported by Grant-in-Aid for Scientific Research (S) No. 15106003, 2004 and the 21st Century COE Research, Center for Atomistic Fabrication Technology, 2004 from the Ministry of Education, Sports, Culture, Science and Technology.

[1] W. Yun *et al.*, Rev. Sci. Instrum. **70**, 2238 (1999).
[2] E. Di Fabrizio, F. Romanato, M. Gentili, S. Cabrini, B. Kaulich, J. Susini, and R. Barrett, Nature (London) **401**, 895 (1999).
[3] C. G. Schroer *et al.*, Appl. Phys. Lett. **82**, 1485 (2003).
[4] K. Yamauchi *et al.*, J. Synchrotron Radiat. **9**, 313 (2002).
[5] Y. Mori *et al.*, Proc. SPIE **5193**, 11 (2003).
[6] O. Hignette, G. Rostaing, P. Cloetens, A. Rommeveaux, W. Ludwig, and A. K. Freund, Proc. SPIE **4499**, 105 (2001).
[7] G. E. Ice, J. S. Chung, J. Z. Tischler, A. Lunt, and L. Assoufid, Rev. Sci. Instrum. **71**, 2635 (2000).
[8] H. Mimura *et al.*, J. Synchrotron Radiat. **11**, 343 (2004).
[9] K. Yamauchi, H. Mimura, K. Inagaki, and Y. Mori, Rev. Sci. Instrum. **73**, 4028 (2002).
[10] K. Yamamura *et al.*, Rev. Sci. Instrum. **74**, 4549 (2003).
[11] K. Yamauchi *et al.*, Jpn. J. Appl. Phys., Part 1 **42**, 7129 (2003).
[12] K. Tamasaku, Y. Tanaka, M. Yabashi, H. Yamazaki, N. Kawamura, M. Suzuki, and T. Ishikawa, Nucl. Instrum. Methods Phys. Res. A **467–468**, 686 (2001).
[13] H. Mimura *et al.*, Rev. Sci. Instrum. **76**, 045102 (2005).
[14] K. Yamauchi *et al.*, Rev. Sci. Instrum. **74**, 2894 (2003).
[15] S. Matsuyama *et al.*, Proc. SPIE **5533**, 181 (2004).